Engineering Structures 308 (2024) 117889

Contents lists available at ScienceDirect

Engineering Structures

journal homepage: www.elsevier.com/locate/engstruct

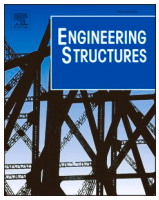

Experimental investigation of the shear force capacity of prismatic cross laminated timber beams

Henrik Danielsson [a,*], Tomaž Pazlar [b], Erik Serrano [a], Boris Azinović [b]

[a] Division of Structural Mechanics, Lund University, P.O. Box 118, Lund SE-221 00, Sweden
[b] Slovenian National Building and Civil Engineering Institute (ZAG), Section for Timber Structures, Dimičeva ulica 12, Ljubljana, Slovenia

ARTICLE INFO

Keywords:
Cross laminated timber
CLT
Beam
Testing
Shear capacity
Shear failure mode III
Design methods

ABSTRACT

Experimental tests of Cross Laminated Timber (CLT) under in-plane beam loading conditions are presented. The influence of the element layup, the individual lamination width, and the beam overhang at the supports on the shear force capacity was investigated. All the CLT beams had the same gross cross section, and a 4-point-bending test setup was used. The experimentally determined load-bearing capacities are compared with the load-bearing capacities resulting from analytical methods proposed for structural design, focusing on shear failure in the crossing areas of flatwise bonded laminations (shear failure mode III). The test results indicate no or very small influence of the element layup and the lamination width on the shear force capacity. These results partly contradict the predictions of the proposed design methods. Of the three studied beam geometry parameters, the beam overhang at the support had the greatest influence on the load-bearing capacity.

1. Background and introduction

The construction sector is responsible for a significant proportion of total greenhouse gas emissions and our negative climate impact. However, advances in modern timber construction and the development of innovative wood-based structural components in recent decades have opened up new opportunities to reduce the carbon footprint of residential, public, office and school buildings. Cross Laminated Timber (CLT) has played an important role in this transition to more sustainable construction, as it is a versatile structural element that can be used for walls, floors, roofs, and beams in load-bearing structures.

For in-plane beam loading, CLT has many inherent positive properties in terms of load-bearing capacity. The crosswise arrangement of the laminations results in considerable strength and stiffness both in the direction parallel to the beam axis and in the direction perpendicular to the beam axis. The comparatively high strength and stiffness under load in the beam height direction, thanks to the transverse laminations, is a major advantage over conventional glulam, especially for beams with irregular geometries, e.g., due to holes, notches, and tapers. However, modelling and predicting the load-bearing capacity of CLT beams is much more complex than for wood-based elements with unidirectional fibre orientation. When considering in-plane shear loading of CLT, three different failure modes (FM) should generally be considered in the design (see Fig. 1): Gross shear failure (I), net shear failure in longitudinal or transverse laminations (II) and shear failure in the crossing areas between bonded laminations of adjacent layers (III).

Several experimental studies on the load-bearing capacity of CLT under in-plane beam loading can be found in the literature. A summary of previous experimental tests is given below and setups, beam geometries and layups used for these tests are shown in Figure A.1 in Appendix A.

Jöbstl et al. [2] report on the testing of CLT beams according to the method of CUAP 03.04/06 [3] with reference to EN 408:2003 [4], using a 4-point-bending test. The CLT beams consisted of longitudinal layers with two laminations in the direction of the beam height, and featured a clear gap between them, to allow for net shear failure of the transverse layers. Seven test series were carried out with 3- and 5-layer CLT beams of different layups, with a total of 90 individual tests. None of the beams failed due to shear and it was concluded that the test configuration is unsuitable for determining the net shear strength properties of CLT.

Tests on self-manufactured CLT beams are reported by Bejtka in [5], which also contains test results for diagonal laminated timber beams. A total of 10 CLT beams were tested in two different 4-point-bending setups, one focusing on bending failure ("long beams", span-to-beam-height ratio $L/h \approx 14.1$) and the other on shear failure ("short beams", $L/h \approx 5.8$). The beams consisted of 5-layer CLT, which had the same element layup in terms of the individual layer thicknesses: 35-17.5-35-17.5-35 (in mm, with transverse layers underlined). All "long beams" failed in bending by fracture of the longitudinal

* Corresponding author.
E-mail address: henrik.danielsson@construction.lth.se (H. Danielsson).

https://doi.org/10.1016/j.engstruct.2024.117889
Received 20 September 2023; Received in revised form 1 March 2024; Accepted 17 March 2024
Available online 5 April 2024

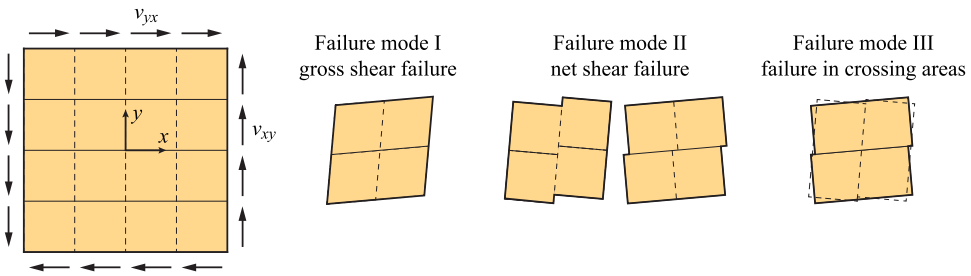

Fig. 1. Failure modes for in-plane shear loading of CLT reproduced from [1].

laminations on the tension side of the beams, between the two point loads. For the "short beams", shear failure, bending failure, and mixed shear/bending failure were reported and the shear failures were characterized by delamination of the outer longitudinal layers.

Further investigations of the in-plane shear strength and stiffness of CLT are presented by Andreolli et al. in [6]. Four test series, with either two or four individual tests within each series, and a total of 10 individual tests were included in that investigation. The number of layers, element layup and the width of the laminations were varied between the test series. The predominant failure mode in the tests was bending. One of the main conclusions from this work was that the standard test configurations according to CUAP 03.04/06 [3] and EN 408:2010 [7] may be unsuitable for obtaining shear induced failures in CLT. The authors also point out that many parameters of the "internal geometry", i.e., the cross-section sizes and the arrangement of the individual laminations, influence the load-bearing capacity.

Extensive experimental tests on CLT under in-plane beam loading have also been published by Flaig in [8–10] and by Flaig & Blass in [11,12]. The tests included prismatic beams and beams with irregularities such as notches, holes, and tapered edges. Prismatic beams with different layups and different number (one to three) of longitudinal laminations in the beam height direction were tested to investigate the system effects on the bending strength. Prismatic 3-layer beams with layups 27-27-27 and 30-20-30 and with two longitudinal laminations in the beam height direction were also tested, using the method of CUAP 03.04/06 [3], with a span-to-beam-height ratio of $L/h = 9$. The failures were due to shear in the crossing areas (FM III) and the mean shear capacity of the beams with the 30-20-30 layup was greater than the mean shear capacity of the beams with the 27-27-27 layup [11].

The tests reported in [13,14] concern both prismatic beams and beams with a hole or notch. A total of 20 tests were carried out on beams with a height of 600 mm, consisting of 5-layer CLT with layup 40-20-40-20-40. Two different 4-point-bending test setups were used to investigate the load-bearing capacity in bending (longer span) and shear (shorter span) for prismatic beams, with four specimens in each test series. The beams were cut from larger CLT panels without considering the arrangement of the individual longitudinal and transverse laminations. The beams with longer span failed in a brittle manner due to bending, at a maximum nominal normal stress of 39.7 MPa (mean value of four tests). The load-bearing capacity of the beams with shorter span was reached at a maximum nominal stress of 36.5 MPa (mean value of four tests) and was preceded by a gradual decrease of the global stiffness. Considerable sliding between adjacent longitudinal laminations was also observed during testing, indicating partial failure of the bonding between longitudinal and transverse layers (FM III). The same type of 4-point-bending test setup was later used to investigate the shear capacity of 3-layer CLT beams with layup 40-20-40, reported in [15]. For these tests, a combination of initial shear failure in the crossing areas (FM III) and final failure due to bending was found. This progressive failure event resulted in a considerable loss in global stiffness during loading. The maximum nominal normal stress at final failure was found to be 25.9 MPa (mean value of four tests).

An analytical model for stress analysis and calculation of the stiffness and load-bearing capacity of CLT beams, concerning failure in bending and shear, has been presented by Flaig & Blass [8,11]. That work formed the basis for the design equations in the Canadian CLT Handbook [16] as well as for the design approach for CLT beams used in earlier drafts of the second-generation of Eurocode 5, see e.g. the overview and discussion in [17] on the development of parts of Eurocode 5 dealing with CLT. The current draft of the new Eurocode 5 [18] does however not contain any specific design equations for CLT beams.

Numerical studies based on 3D Finite Element (FE) analyses of the internal force and stress distribution have revealed discrepancies with respect to the assumptions of the model presented by Flaig & Blass, see e.g. [14,19,20]. The discrepancies between the numerical results and the assumptions of the analytical model relate to the predicted magnitudes of the torsional moments and shear forces acting in the crossing areas between the flatwise bonded laminations of adjacent layers, as well as to their distribution in the directions of the beam height and width. These torsional moments and shear forces are decisive for the prediction of the load-bearing capacity in relation to shear FM III.

Several approaches have also been proposed for prediction of shear stresses in the crossing areas of CLT under pure in-plane shear loading, see e.g. [1] for an overview. However, the stress states differ slightly between the case of pure in-plane shear loading and the case of in-plane beam loading. Under pure in-plane shear loading, the shear stresses in the crossing areas can be considered as a result of pure torsion. In the case of in-plane beam loading, the shear stresses in the crossing areas are due to a combination of torsion and shear forces in the directions parallel and perpendicular to the beam axis. Modifications and improvements of the model by Flaig & Blass [8,11] are proposed in [15,19,21], in order to achieve a better agreement between the predictions of the analytical model and the numerical results for the torsional moments and shear forces in the crossing areas of CLT beams. This modified model for stress predictions, and related to the shear capacity of CLT beams, is further discussed in [20]. There, a unified design approach for in-plane beam loading and pure in-plane shear loading is also proposed, taking into account the models for pure shear presented in [1,22].

Thus, there are two slightly different approaches for stress predictions related to shear FM III for CLT beams:

- Model of Flaig & Blass (Canadian CLT Handbook, earlier drafts of the new Eurocode 5)
- Model of Danielsson, Jeleč, Rajčić & Serrano

As described above, several test campaigns of CLT under in-plane beam loading conditions are reported in the literature. However, these campaigns are usually limited to consideration of a single element layup, i.e., no variation of the individual layer thicknesses between the test series or limited to test series with very few nominally equal specimens.

In order to evaluate the two aforementioned approaches for stress prediction in relation to shear failure mode III and the corresponding load-bearing capacity, a test programme (see Figs. 2 and 3) was

developed to allow the influence of the following two parameters on the response to be investigated:

- Ratio of the longitudinal layers' thicknesses
- Lamination widths

In addition, the experimental tests included studies on a third parameter:

- Beam geometry in terms of the overhang at the support

As far as the authors are aware, structured experimental studies of these three parameters have not been presented in the research literature.

The present experimental tests and models for stress prediction, including failure criteria, are presented in Section 2. The tests are presented in Section 2.1 in terms of test configuration, material and loading protocol. Approaches for stress analysis according to the model of Flaig & Blass and according to the model of Danielsson, Jeleč, Rajčić & Serrano are reviewed in Section 2.2. Experimental results and comparisons with analytical model predictions are presented in Section 3. The discussion of the results is presented in Section 4 and the conclusions are presented in Section 5.

2. Materials and methods

2.1. Experimental tests

The experiments were conducted at the Slovenian National Building and Civil Engineering Institute (ZAG), where 5-layer CLT beams were loaded using a 4-point-bending test setup as shown in Fig. 2. The test programme consisted of six test series with six beam specimens within each test series according to Table 1, resulting in a total of 36 individual tests. The gross cross-section was the same for all beams: $t_{gross} = 140$ mm and $h = 600$ mm. All element layups were symmetrical in the direction of the beam width and the transverse layer thicknesses were consistently $t_{y,1} = 20$ mm, resulting in a net cross-section thickness of the transverse layers, t_y, of 40 mm. The net cross-section thickness of the longitudinal layers, t_x, was kept constant at 100 mm, while the thicknesses of the individual longitudinal layers were varied between the test series.

Three different element layups were tested:

- Layup A: 40-20-20-20-40
- Layup B: 33-20-34-20-33
- Layup C: 25-20-50-20-25

as shown in Fig. 3 and with transverse layer thicknesses underlined. The layups result in ratios between internal and external longitudinal layer thicknesses of $t_{x,2}/t_{x,1} = 0.5$, 1.0 and 2.0 for layups A, B and C, respectively. The lamination widths $b_x = b_y = 100$ mm and $b_x = b_y = 150$ mm were investigated for each layup. Within each test series, three beams had an overhang at the supports of $L_e = 400$ mm and three beams had an overhang of $L_e = 120$ mm, cf. Fig. 2.

The CLT beams were manufactured by LIGNOTREND GmbH in accordance with AbZ Z-9.1–555 [23], with timber laminations made of Norway spruce (*Picea abies*) and corresponding to strength class C24 according to the European standard EN 338 [24]. The elements were manufactured using a one-component polyurethane adhesive for the flat-side bonding and without edge-bonding between the laminations within the same layer. The specimens were not conditioned prior to testing and the moisture content at the time of testing was measured according to EN 13183–2 [25], resulting in an average moisture content of 13.6% (CoV 16.2%). The mean density of the test specimens was 464 kg/m^3 (CoV 3.6%). The results presented in Section 3 contain both data as measured during testing and data obtained by adjustments of data for variations in moisture content.

In specimens with $b_x = 100$ mm, some individual laminations of the outer CLT layers exhibited a small curvature. In some extreme cases, this led to the formation of gaps along the narrow edge of the laminations with a width of up to 10 mm, but only at the location of the beam support and not over the entire length of the beam. The analysis of the failure modes does not indicate that these gaps had any influence on the test results.

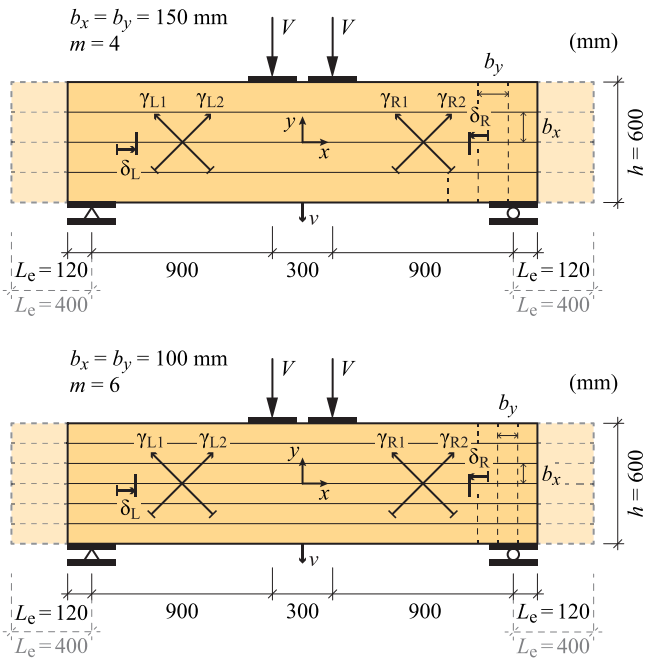

Fig. 2. Test setup and beam geometries.

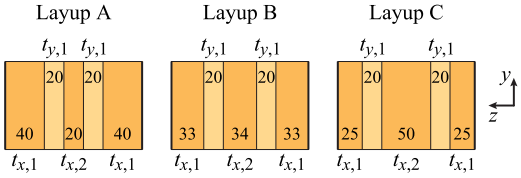

Fig. 3. CLT element layups A, B and C, with layer thicknesses in mm.

The load was applied displacement-controlled with a single 500 kN actuator (MTS 661.23 H-01) and a load rate of 0.03 mm/s. The average time to reach the maximum load was 795 s (with a maximum time of 1389 s and a minimum time of 540 s), considering all 36 individual tests. Steel plates with a length of 240 mm were used at the supports and at the points of load introduction, as shown in Fig. 2. The beams were restrained from lateral movement in the out-of-plane direction at the two supports and at the beam midspan.

Relative displacements were measured with seven potentiometric displacement transducers at the locations shown in Fig. 2, with a measuring range of 25 mm or 100 mm and an accuracy of ≤ 0.05 mm or ≤ 0.1 mm, respectively. The beam deflection (v) measurements were taken at the bottom of the beam at midspan. Deformation measurements were also taken over two pairs of crosswise arranged diagonals (γ_{L1}-γ_{L2} and γ_{R1}-γ_{R2}), to assess the shear stiffness in accordance with the procedure of the shear field test method in the European standard EN 408 [26]. The relative slip (δ_L and δ_R) in the longitudinal direction of the beam between the two most centrally placed laminations in the beam height direction was also measured, between the load introduction points and the supports on both sides of the beam for the view shown in Fig. 2.

In addition, the other side of each beam was monitored with a Digital Image Correlation (DIC) system, Aramis GOM 5M. The measurements were performed in 2D with two cameras, each camera imaging a field of approximately 0.65 × 0.60 m on the left and right side from the load insertion points in the centre of the beam (see also Fig. 8). During the tests, images with a resolution of 2448 × 2050 pixels were captured every two seconds. In this way, a measurement accuracy of approximately ± 0.005 mm was achieved in the in-plane directions.

Table 1
Description of test series geometry parameters, density ρ, and moisture content u.

Specimen	$b_x = b_y$ (mm)	$t_{x,1}$ (mm)	$t_{y,1}$ (mm)	$t_{x,2}$ (mm)	$t_{y,1}$ (mm)	$t_{x,1}$ (mm)	L_e (mm)	ρ (kg/m^3)	u (%)
A-100-1	100	40	20	20	20	40	400	488	13.7
A-100-2	100	40	20	20	20	40	400	490	14.3
A-100-3	100	40	20	20	20	40	400	472	11.3
A-100-4	100	40	20	20	20	40	120	474	11.8
A-100-5	100	40	20	20	20	40	120	473	11.5
A-100-6	100	40	20	20	20	40	120	490	10.9
A-150-1	150	40	20	20	20	40	400	477	13.5
A-150-2	150	40	20	20	20	40	400	471	12.2
A-150-3	150	40	20	20	20	40	400	480	11.5
A-150-4	150	40	20	20	20	40	120	463	12.5
A-150-5	150	40	20	20	20	40	120	464	12.5
A-150-6	150	40	20	20	20	40	120	460	14.0
B-100-1	100	33	20	34	30	33	400	457	15.4
B-100-2	100	33	20	34	30	33	400	468	17.5
B-100-3	100	33	20	34	30	33	400	461	16.4
B-100-4	100	33	20	34	30	33	120	446	15.9
B-100-5	100	33	20	34	30	33	120	435	14.0
B-100-6	100	33	20	34	30	33	120	447	16.1
B-150-1	150	33	20	34	30	33	120	466	16.0
B-150-2	150	33	20	34	30	33	120	451	16.7
B-150-3	150	33	20	34	30	33	120	468	15.2
B-150-4	150	33	20	34	30	33	400	456	17.8
B-150-5	150	33	20	34	30	33	400	475	16.1
B-150-6	150	33	20	34	30	33	400	475	17.4
C-100-1	100	25	20	50	20	25	400	412	12.7
C-100-2	100	25	20	50	20	25	400	452	12.5
C-100-3	100	25	20	50	20	25	400	452	12.4
C-100-4	100	25	20	50	20	25	120	460	13.1
C-100-5	100	25	20	50	20	25	120	446	12.8
C-100-6	100	25	20	50	20	25	120	446	13.4
C-150-1	150	25	20	50	20	25	400	466	10.6
C-150-2	150	25	20	50	20	25	400	472	11.8
C-150-3	150	25	20	50	20	25	400	465	11.0
C-150-4	150	25	20	50	20	25	120	503	10.3
C-150-5	150	25	20	50	20	25	120	465	12.5
C-150-6	150	25	20	50	20	25	120	458	10.5

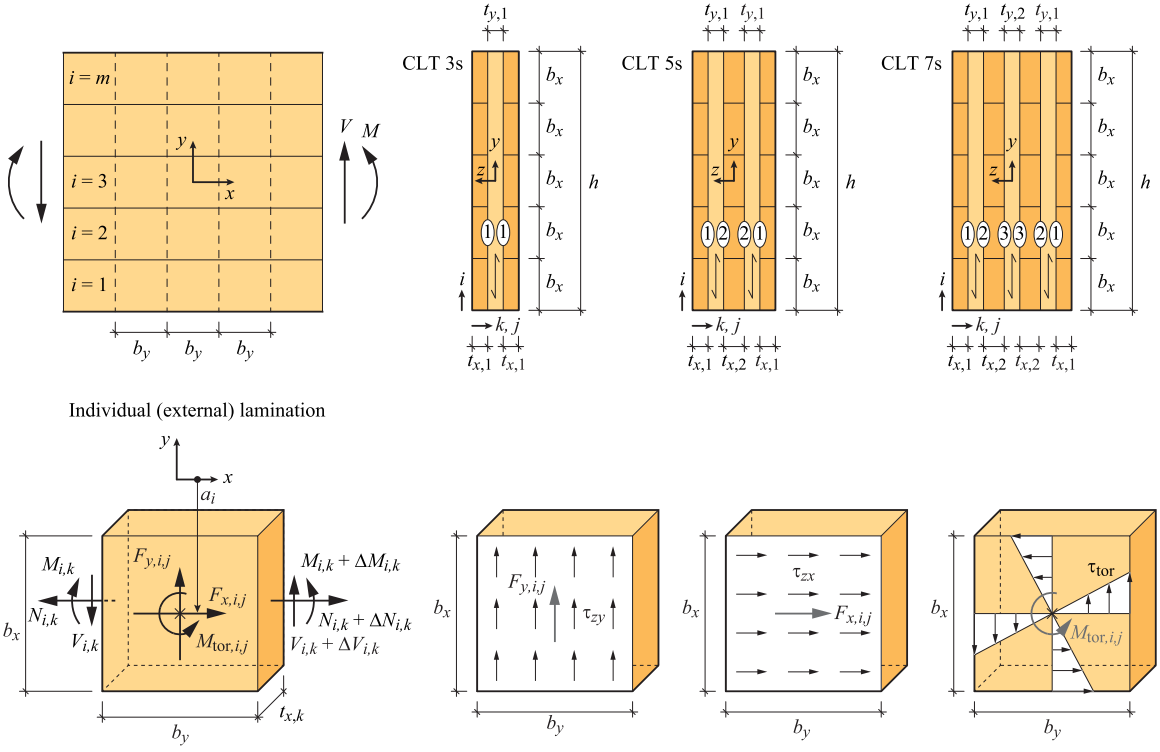

Fig. 4. Illustration of beam model and definition of load and geometry parameters, under the CC BY-NC-ND license. reproduced from [20]

2.2. Models for prediction of stresses and load-bearing capacity

Equations making it possible to express the test results in terms of stresses that are relevant for bending and shear failure modes are presented below. The notations for loads, stresses and beam geometry parameters are shown in Fig. 4.

The index i refers to the position of the longitudinal laminations and crossing areas in the beam height direction. Index k refers to the position of the longitudinal laminations in the beam width direction and index j refers to the position of the crossing areas in the beam width direction. The models and equations stated below are generally based on the assumption of equal laminations widths b_x for all longitudinal laminations, resulting in $h = mb_x$, where m is the number of laminations in the beam height direction.

The maximum nominal normal stress σ_x due to bending is defined as

$$\sigma_x = \frac{6M}{t_x h^2} \tag{1}$$

where M refers to the bending moment ($M_{\max} = 1.5Vh$ for the present test setup), $t_x = \Sigma t_{x,k}$ is the total net cross-section thickness of the longitudinal layers and where h is the beam height.

The gross shear stress is defined by

$$\tau_{xy,\text{gross}} = \frac{3}{2}\frac{V}{t_{\text{gross}} h} \tag{2}$$

where V refers to the shear force and where t_{gross} refers to the total gross cross-section thickness.

The net shear stress in the transverse layers is defined by

$$\tau_{xy,\text{net}} = \frac{3}{2}\frac{V}{t_y h} \tag{3}$$

where t_y refers to the total net cross-section thickness of the transverse layers. Only the net shear stress in the transverse layers is considered here, as the net cross-section thickness of the transverse layers (t_y = 40 mm) is much smaller than net cross-section thickness of the longitudinal layers (t_x = 100 mm).

For verification of the load-bearing capacity with respect to shear failure mode III, failure in the crossing areas, the two models considered are formulated in terms of two stress components: the shear stress τ_{zx} parallel to the beam axis and a torsional shear stress τ_{tor}. Both models are based on the assumption of linear elastic behaviour and the distribution of shear stresses over the crossing areas as shown in Fig. 4. The failure criterion for shear failure mode III, proposed in [8,11], is given by

$$\frac{\tau_{zx}}{f_r} + \frac{\tau_{\text{tor}}}{f_{v,\text{tor}}} \le 1.0 \tag{4}$$

where f_r is the rolling shear strength of the laminations and where $f_{v,\text{tor}}$ is a torsional shear strength parameter.

According to the model presented in [8,11], and its implementation in earlier drafts of the second-generation of Eurocode 5 and in the Canadian CLT Handbook [16], the design-relevant shear stress components can, with sufficient accuracy, be expressed as

$$\tau_{zx} = \frac{6V}{b_x^2}\frac{1}{n_{\text{CA}}}\left(\frac{1}{m^2} - \frac{1}{m^3}\right) \tag{5}$$

and

$$\tau_{\text{tor}} = \frac{3V}{b_x^2}\frac{1}{n_{\text{CA}}}\left(\frac{1}{m} - \frac{1}{m^3}\right)k_b \text{ with } k_b = \frac{2b_{\max}b_x}{b_x^2 + b_y^2} \tag{6}$$

and where n_{CA} is the total number of crossing areas in the beam width direction and where $b_{\max} = \max\{b_x, b_y\}$. The notation used in Eqs. (5) and (6) has been slightly changed compared to [8,11] and [16], for consistency within the present paper.

Eqs. (5) and (6) are based on the assumption of equal stress states for all crossing areas in the beam width direction, for longitudinal laminations at the same position in the beam height direction, i.e., at the same location i. In the derivation, it is also assumed that the torsional moments $M_{\text{tor},i,j}$, which result in the torsional shear stress τ_{tor}, are the same for all crossing areas in the beam height direction. Eq. (5) refers to the shear stress τ_{zx} in the uppermost and lowermost crossing area with respect to the beam height direction, where (due to equilibrium considerations) the maximum shear stresses parallel to the beam axis are found. Therefore, the critical (most stressed) crossing area in relation to shear failure mode III, according to the criterion in Eq. (4) with stresses according to Eqs. (5) and (6), are the upper/lowermost crossing areas in the beam height direction.

In the model by Danielsson et al. [15,19–21], slightly different internal force and stress distributions are found from equilibrium considerations. A non-uniform distribution of the torsional moments $M_{\text{tor},i,j}$ in the beam height direction is recognised and crossing area shear stresses are in this model influenced by the element layup in terms of the individual thicknesses of the respective layers, i.e., by the ratios $t_{x,k}/t_x$ and $t_{y,k}/t_y$.

The shear stress parallel to the beam axis, acting in a crossing area with location i,j as shown in Fig. 4 may according to [19,20] for 5-layer CLT beams be expressed as

$$\tau_{zx,i,j} = \frac{12V}{h^3}\frac{1}{n_{\text{CA},k}}\frac{t_{x,k}}{t_x}a_i \tag{7}$$

where $j = k = 1$ or 2 and where a_i is the distance from the centre axis of the CLT beam gross cross-section to the centre axis of an individual longitudinal lamination i, $t_{x,k}$ is the thickness of longitudinal layer k, and $n_{\text{CA},k}$ is the number of crossing areas that the longitudinal layer k shares with adjacent transverse layers. The maximum stress is found in the uppermost and lowermost crossing area (at maximum distance $a_i = a_1 = a_m$), which is consistent with the location of the maximum stress from the model that yields Eq. (5).

The torsional shear stress component at location i,j as shown in Fig. 4 may according to [19,20] for 5-layer CLT beams be expressed as

$$\tau_{\text{tor},i,j} = \frac{3V}{b_x^2}\frac{1}{n_{\text{CA},k}}\frac{t_{x,k}}{t_x}\left(\alpha_i - \frac{b_x^3}{h^3}\right)k_b \quad \text{where } \alpha_i = \frac{6i - 6i^2 + m(6i-3) - 2}{m^3} \tag{8}$$

and with k_b according to Eq. (6). This model yields maximum torsional moments and corresponding shear stresses for crossing areas at the beam centreline.

The maximum stress values according to Eqs. (7) and (8) generally refer to different crossing areas i in the beam height direction, and the location of the critical crossing area (i.e., the most stressed crossing area) based on the failure criterion in Eq. (4) is not obvious. Moreover, the location of the critical crossing area depends not only on the maximum stress values but also on the respective strength values, i.e. f_r and $f_{v,\text{tor}}$.

Assuming a ratio of strength values of $f_{v,\text{tor}}/f_r = 3.5/1.5 \approx 2.3$, which is based on typical mean strength values found from tests on individual crossing areas loaded in either pure torsion or pure shear, [15] shows that the model predicts the critical crossing area to be at the beam centreline. For this location, the design-relevant stresses according to Eqs. (7) and (8) for 5-layer CLT beams with $j = k = 1$ or 2 can be simplified to

$$\tau_{zx,j} = \frac{6Vb_x}{h^3}\frac{1}{n_{\text{CA},k}}\frac{t_{x,k}}{t_x} \tag{9}$$

and

$$\tau_{\text{tor},j} = \frac{3V}{b_x^2}\frac{1}{n_{\text{CA},k}}\frac{t_{x,k}}{t_x}\left(\frac{3}{2}\frac{b_x}{h} - \frac{b_x^3}{h^3}\right)k_b \tag{10}$$

by approximating the maximum distance from the centreline of the beam to the centre of the critical crossing area as $a_i = b_x/2$ and by an approximation according to $\max\{\alpha_i\} \approx 1.5b_x/h$, as shown in [20].

3. Test results

The individual test results in terms of the maximum shear force reached during loading, V_{max}, and the corresponding stress components according to the analytical models presented in Section 2.2 are given in Table 2. The stress components are determined based on the respective equations as given in the table. Three models are considered for the calculation of the shear stress components τ_{zx} and τ_{tor}, acting in the crossing areas:

- Model 1: Eqs. (5) and (6) according to the model by Flaig & Blass.
- Model 2: Eqs. (7) and (8) according to the model by Danielsson et al.
- Model 3: Eqs. (9) and (10) according to simplifications of Model 2.

For all three models, Table 2 also gives a utilisation ratio for shear failure mode III according to the failure criterion given in Eq. (4). This ratio is based on the assumed mean strength values of $f_r = 1.5$ MPa and $f_{v,tor} = 3.5$ MPa, as indicated by the compilations of test results for individual crossing areas subjected to either pure uniaxial shear or pure torsion presented in [8,15].

The individual test results in terms of shear force V vs. beam midspan displacement v are shown in Fig. 5. All tests show a nonlinear load-displacement response, to varying degree, before the maximum load, V_{max}, is reached. To allow further comparison of the test results, a load level V_{init} was introduced that corresponds to the initiation of this nonlinear phase. This load level was defined as the shear force at which the tangent stiffness k_{init} is 80% of the initial stiffness k_0, i.e., a 20% reduction. The stiffness k_0 was in turn defined from measurement points within the range $0.10V_{max} \leq V \leq 0.40V_{max}$ and determined on the basis of a linear regression. The tangential stiffness k_{init} was also determined on the basis of a linear regression, from data points within a range of $V = \pm 0.05V_{max}$ at the considered load level. The criteria for determination of k_{init} are not standardised and therefore different reduction factors were analysed, ranging from 5% to 40% reduction of k_0. The study showed that the influence on the result trends was very small and therefore only values for a 20% reduction in stiffness are shown in this article. The load

Table 2
Test results for individual specimens in terms of shear force at initiation of nonlinear response, V_{init}, maximum shear force, V_{max}, and stress components at V_{max}, according to *Section* 2.2.

						Model 1 – Flaig/Blass			Model 2 – Danielsson et al.			Model 3 – Design proposal		
			Eq. (1)	Eq. (2)	Eq. (3)	Eq. (5)	Eq. (6)	Eq. (4)	Eq. (7)	Eq. (8)	Eq. (4)	Eq. (9)	Eq. (10)	Eq. (4)
Specimen	V_{init} (kN)	V_{max} (kN)	σ_x (MPa)	$\tau_{xy,gross}$ (MPa)	$\tau_{xy,net}$ (MPa)	τ_{zx} (MPa)	τ_{tor} (MPa)	Ratio (-)	τ_{zx} (MPa)	τ_{tor} (MPa)	Ratio (-)	τ_{zx} (MPa)	τ_{tor} (MPa)	Ratio (-)
A-100-1	189.3	225.3	32.4	3.85	13.5	0.782	2.74	130%	0.250	6.38	199%	0.250	6.63	206%
A-100-2	158.7	224.8	33.7	4.01	14.0	0.781	2.73	130%	0.250	6.37	199%	0.250	6.62	206%
A-100-3	145.6	211.3	31.7	3.77	13.2	0.734	2.57	122%	0.235	5.99	187%	0.235	6.22	193%
A-100-4	136.1	189.7	28.5	3.39	11.9	0.659	2.31	110%	0.211	5.37	168%	0.211	5.58	174%
A-100-5	157.6	214.5	32.2	3.83	13.4	0.745	2.61	124%	0.238	6.08	190%	0.238	6.32	196%
A-100-6	141.7	216.5	32.5	3.87	13.5	0.752	2.63	125%	0.241	6.13	191%	0.241	6.37	198%
Mean	**154.8**	**213.7**	**31.8**	**3.79**	**13.3**	**0.742**	**2.60**	**124%**	**0.237**	**6.05**	**189%**	**0.237**	**6.29**	**196%**
CoV	**12.3%**	**6.1%**												
A-150-1	132.6	208.7	31.3	3.73	13.0	0.652	1.63	90%	0.348	3.65	128%	0.348	4.00	137%
A-150-2	147.4	227.1	34.1	4.06	14.2	0.710	1.77	98%	0.378	3.97	139%	0.378	4.35	150%
A-150-3	155.6	218.6	32.8	3.90	13.7	0.683	1.71	94%	0.364	3.83	134%	0.364	4.19	144%
A-150-4	130.4	191.3	28.7	3.42	12.0	0.598	1.49	83%	0.319	3.35	117%	0.319	3.67	126%
A-150-5	150.3	196.4	29.5	3.51	12.3	0.614	1.53	85%	0.327	3.44	120%	0.327	3.76	129%
A-150-6	123.0	180.8	27.1	3.23	11.3	0.565	1.41	78%	0.301	3.16	111%	0.301	3.47	119%
Mean	**139.9**	**203.8**	**30.6**	**3.64**	**12.7**	**0.637**	**1.59**	**88%**	**0.340**	**3.57**	**125%**	**0.340**	**3.91**	**134%**
CoV	**9.3%**	**8.6%**												
B-100-1	139.7	212.1	31.8	3.79	13.3	0.736	2.58	123%	0.194	4.96	155%	0.194	5.15	160%
B-100-2	141.9	214.2	32.1	3.82	13.4	0.744	2.60	124%	0.196	5.01	156%	0.196	5.20	162%
B-100-3	145.7	218.0	32.7	3.89	13.6	0.757	2.65	126%	0.200	5.09	159%	0.200	5.29	165%
B-100-4	152.4	196.6	29.5	3.51	12.3	0.683	2.39	114%	0.180	4.60	143%	0.180	4.78	148%
B-100-5	141.9	201.1	30.2	3.59	12.6	0.698	2.44	116%	0.184	4.70	147%	0.184	4.89	152%
B-100-6	141.2	207.2	31.1	3.70	12.9	0.719	2.52	120%	0.190	4.84	151%	0.190	5.03	156%
Mean	**143.8**	**208.2**	**31.2**	**3.72**	**13.0**	**0.723**	**2.53**	**120%**	**0.191**	**4.87**	**152%**	**0.191**	**5.06**	**157%**
CoV	**3.2%**	**3.9%**												
B-150-1	146.7	191.4	28.7	3.42	12.0	0.598	1.50	83%	0.263	2.76	97%	0.263	3.03	104%
B-150-2	138.4	172.4	25.9	3.08	10.8	0.539	1.35	74%	0.237	2.49	87%	0.237	2.73	94%
B-150-3	146.0	202.3	30.4	3.61	12.6	0.632	1.58	87%	0.278	2.92	102%	0.278	3.20	110%
B-150-4	156.7	214.2	32.1	3.82	13.4	0.669	1.67	92%	0.295	3.09	108%	0.295	3.39	116%
B-150-5	144.8	208.9	31.3	3.73	13.1	0.653	1.63	90%	0.287	3.02	105%	0.287	3.30	114%
B-150-6	153.7	221.1	31.7	3.77	13.2	0.691	1.73	95%	0.304	3.05	111%	0.304	3.50	120%
Mean	**147.7**	**201.7**	**30.0**	**3.57**	**12.5**	**0.630**	**1.58**	**87%**	**0.277**	**2.89**	**102%**	**0.277**	**3.19**	**110%**
CoV	**4.4%**	**8.7%**												
C-100-1	145.0	210.2	31.5	3.75	13.1	0.730	2.55	122%	0.146	3.72	116%	0.146	3.87	120%
C-100-2	158.3	215.0	32.3	3.84	13.4	0.747	2.61	124%	0.149	3.81	119%	0.149	3.96	123%
C-100-3	160.8	203.0	30.5	3.63	12.7	0.705	2.47	117%	0.141	3.60	112%	0.141	3.74	116%
C-100-4	142.1	205.9	30.9	3.68	12.9	0.715	2.50	119%	0.143	3.65	114%	0.143	3.79	118%
C-100-5	142.1	182.8	27.4	3.26	11.4	0.635	2.22	106%	0.127	3.24	101%	0.127	3.36	105%
C-100-6	147.0	190.0	28.5	3.39	11.9	0.660	2.31	110%	0.132	3.36	105%	0.132	3.50	109%
Mean	**149.2**	**201.2**	**30.2**	**3.59**	**12.6**	**0.698**	**2.44**	**116%**	**0.140**	**3.56**	**111%**	**0.140**	**3.70**	**115%**
CoV	**5.5%**	**6.1%**												
C-150-1	138.6	218.1	32.7	3.89	13.6	0.682	1.70	94%	0.227	2.39	83%	0.227	2.61	90%
C-150-2	150.0	195.6	29.3	3.49	12.2	0.611	1.53	84%	0.204	2.14	75%	0.204	2.34	81%
C-150-3	149.6	214.5	32.2	3.83	13.4	0.670	1.68	93%	0.223	2.35	82%	0.223	2.57	88%
C-150-4	146.5	180.0	27.0	3.21	11.2	0.562	1.41	78%	0.187	1.97	69%	0.187	2.16	74%
C-150-5	144.9	179.8	27.0	3.21	11.2	0.562	1.40	78%	0.187	1.97	69%	0.187	2.15	74%
C-150-6	141.6	181.0	27.2	3.23	11.3	0.566	1.41	78%	0.189	1.98	69%	0.189	2.17	75%
Mean	**145.2**	**194.8**	**29.2**	**3.48**	**12.2**	**0.609**	**1.52**	**84%**	**0.203**	**2.13**	**74%**	**0.203**	**2.33**	**80%**
CoV	**3.1%**	**9.1%**												

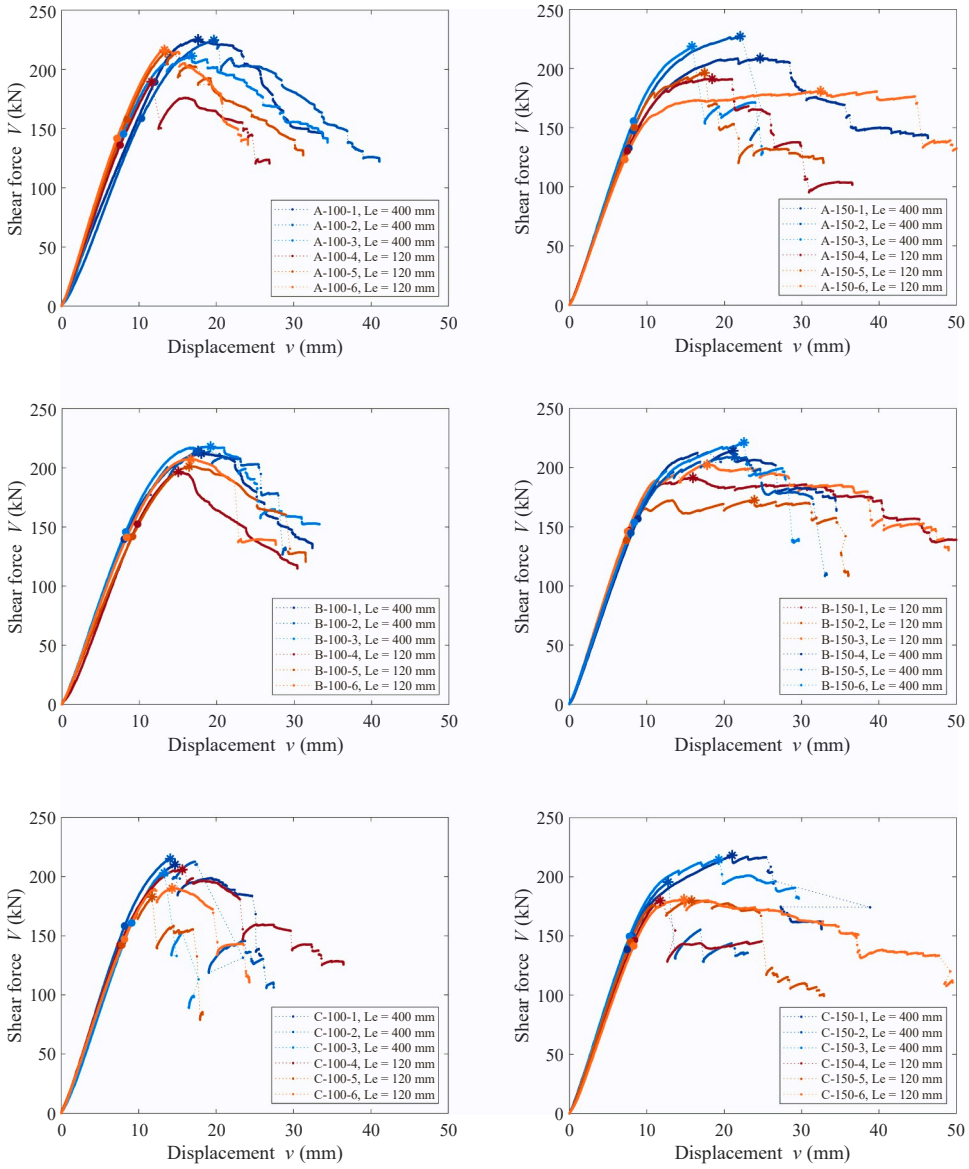

Fig. 5. Shear force V vs. beam midspan displacement v for the six test series, with test specimen notation and the length of the beam overhang at support (L_e) given in the respective legends. Solid circles represent the load level V_{init} and stars represent V_{max}.

levels V_{init} and V_{max} were used as two alternative definitions of the shear capacity, when comparing the different test series and when comparing the experimental results with the predicted capacities according to the analytical models presented in Section 2.2.

The final failures in all tests were bending failures. These were characterised by cracking and failure of the laminations on the lower (tension) side of the beam and/or bending failure of several individual longitudinal laminations in the direction of the beam height. During the tests, significant sliding between adjacent longitudinal laminations occurred, before the maximum load was reached, see Fig. 6. Partial failure of the crossing areas between laminations of adjacent layers was also observed at the end-faces of the beams, see Fig. 7. Sliding between longitudinal laminations can also be seen in Fig. 8, which shows the engineering shear strains (γ_{xy}) measured on the surface with DIC at four load levels for one of the beam specimens. This indicates that severe damage and partial failure due to shear stresses occurred over the crossing areas (FM III) before final failure due to bending was reached. The specimens were not opened after testing and possible damage/failure of the internal transverse laminations in FM II cannot be excluded, although such damage is judged unlikely.

The effective shear modulus, G_{ef}, was assessed from the deformation measurements over the two pairs of crosswise arranged diagonals, see γ_{L1}-γ_{L2} and γ_{R1}-γ_{R2} in Fig. 2. The effective shear modulus was determined as $G_{ef} = \tau_{mean}/\gamma_{mean}$, where τ_{mean} is the mean shear stress over the measurement height (assuming a parabolic shear stress distribution) and where γ_{mean} is determined from the deformations of the two diagonals within the range $0.10V_{max} \leq V \leq 0.40V_{max}$ on the basis of a linear regression. The mean effective shear modulus for the test series with lamination width $b = 150$ mm was found to be very similar for the three layups: $G_{ef} = 505$ MPa, 509 MPa and 497 MPa for test series A-150, B-150, and C-150, respectively. Lower values were found for the lamination width $b = 100$ mm: $G_{ef} = 367$ MPa, 402 MPa and 415 MPa for test series A-100, B-100, and C-100, respectively. The test results did not suggest any influence of the beam overhang length on the effective shear modulus. The results for the effective shear modulus given above have not been adjusted for variations in moisture content.

The moisture content u at the time of testing varies between the individual specimens, see Table 1. The load-bearing capacities in terms of the load levels V_{init} and V_{max} versus the moisture content u for the individual tests are given in Fig. 9, differentiated by the three layups (A, B and

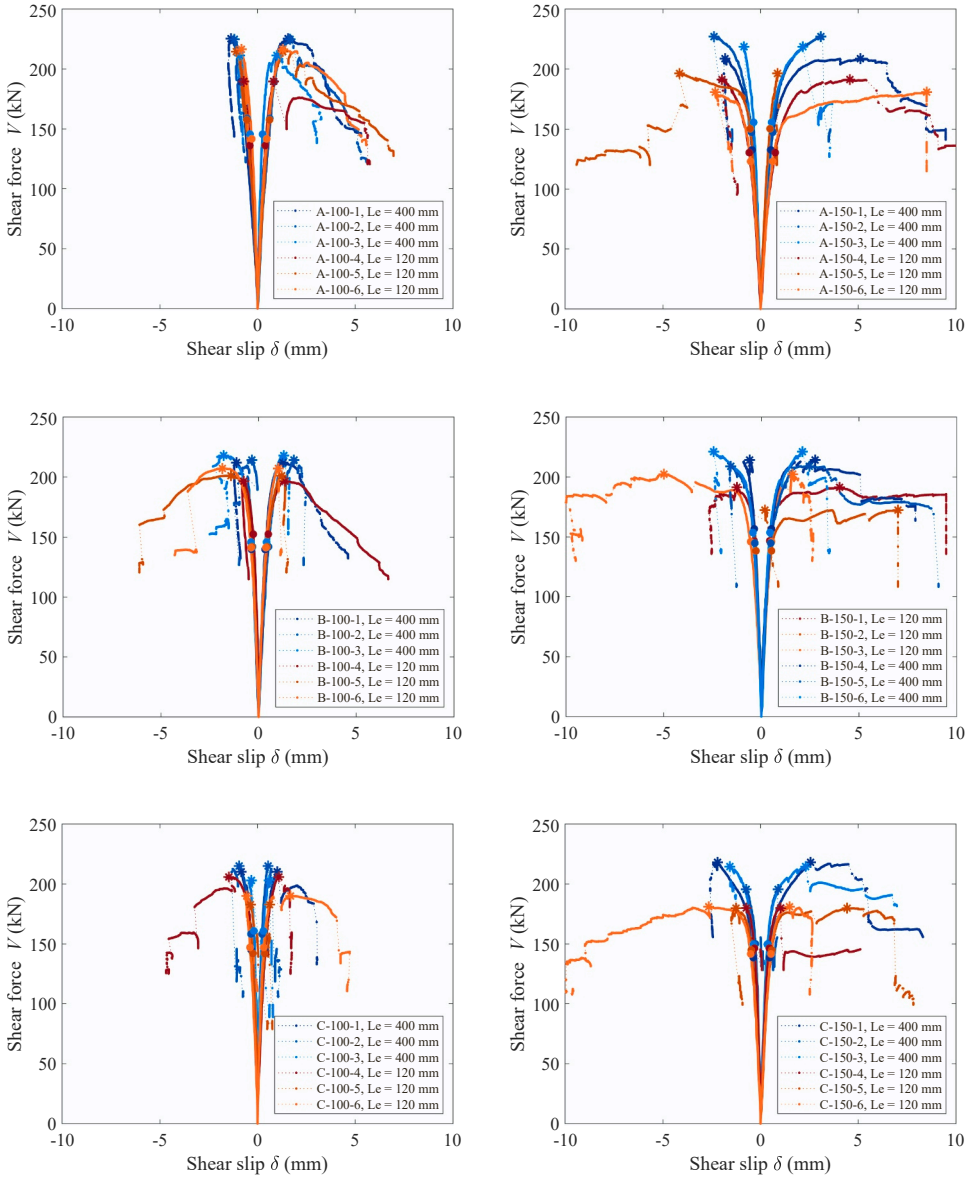

Fig. 6. Shear force V vs. shear slip δ between longitudinal laminations for the six test series, with test specimen notation and the length of the beam overhang at support (L_e) given in the respective legends. Solid circles represent the load level V_{init} and stars represent V_{max}.

C). The load levels V_{max} and V_{init} for all tests are also shown graphically in Fig. 10, where the mean values of the test series and the mean values for the respective subgroups with different lengths of the overhang at the support (L_e) are also shown. Results in Fig. 10a) refer to values of V_{max} and V_{init} as measured during testing and as reported in Table 2.

Shear strength properties have in previous studies shown to be influenced by moisture content. Test results compiled by Brandner et al. [27], suggest a reduction of about 3% for the longitudinal shear strength per each percentage increase in moisture content. For the present application involving shear over crossing areas in CLT, rolling shear strength properties are however more relevant. Akter et al. [28] report on tests of clear wood specimens of Norway spruce loaded in rolling shear at different moisture contents. The results from that study suggest a reduction of about 2% for the rolling shear strength per each percentage increase in moisture content for the interval $9\% < u < 19\%$.

Assuming that the load-bearing capacity has a linear dependency to the moisture content, with a 2% reduction for each percentage increase in moisture content (as indicated in [28]), the shear force load levels V_{max} and V_{init} can be adjusted to levels corresponding to a reference moisture content of $u_{ref} = 12\%$. Such adjusted values, $V_{max,12\%}$ and $V_{init,12\%}$, are shown in Fig. 10b) for all individual tests, which can be compared with the unadjusted test data given in Fig. 10a). Both load levels are adjusted in the same manner, i.e. based on a linear dependency to the moisture content and based on values of V_{max} and V_{init} as given in Table 2 and moisture contents as given in Table 1. The mean values of the moisture content were 12.3%, 12.7%, 12.8% and 11.1% for test series A-100, A-150, C-100 and C-150, respectively. The results for V_{max} and V_{init} for these four test series are hence not influenced much by adjustment to a reference level of $u_{ref} = 12\%$. The mean values of the moisture content for the test series with layup B were slightly higher, 15.9% for B-100 and 16.5% for B-150, and the adjusted load levels V_{max} and V_{init} are hence increased by about 8% for these two test series.

Looking at the maximum shear force, V_{max}, all mean values for the subgroups with a long overhang at the support ($L_e = 400$ mm) are greater than the corresponding mean values for the subgroups with a short overhang at the support ($L_e = 120$ mm), both when considering the measured values of the shear force, see Fig. 10a), and when considering values adjusted to a reference moisture content of 12%, see Fig. 10b).

In the following presentation of test results and comparisons to model predictions, values for shear forces $V_{max,12\%}$ and $V_{init,12\%}$ based on

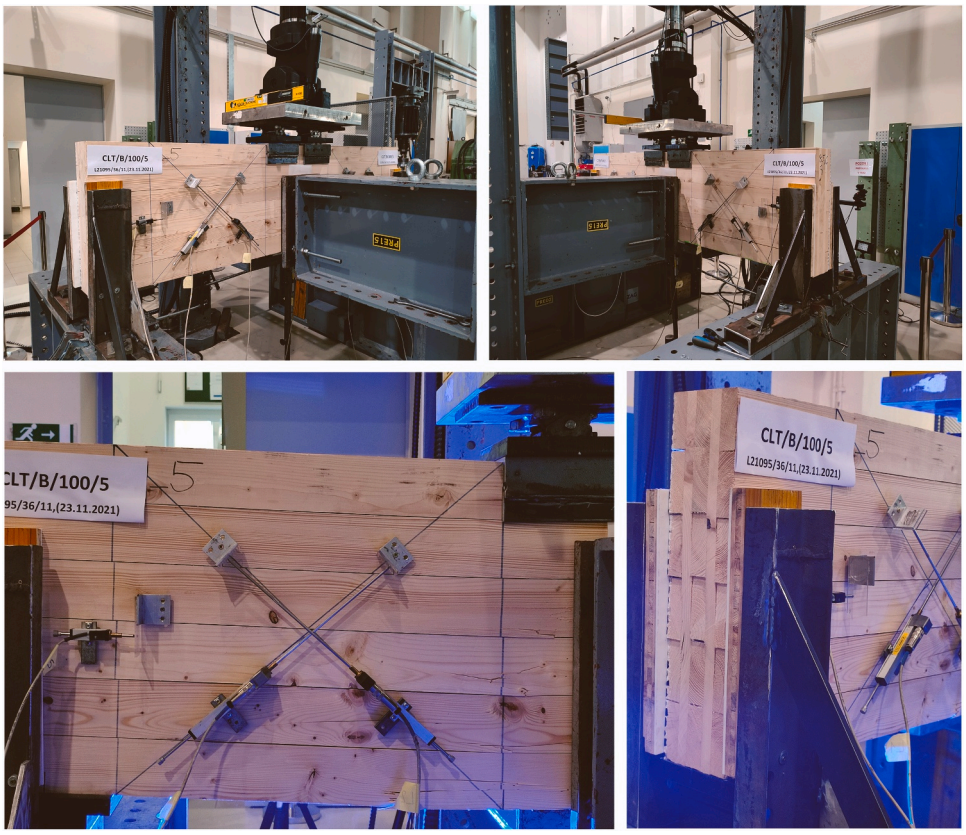

Fig. 7. Testing of specimen B-100-5 (top left and right) and final failure, showing significant sliding between longitudinal laminations and lamination bending failures (bottom left) and the resulting mismatch of lamination ends due to the shear failure of the crossing areas (bottom right).

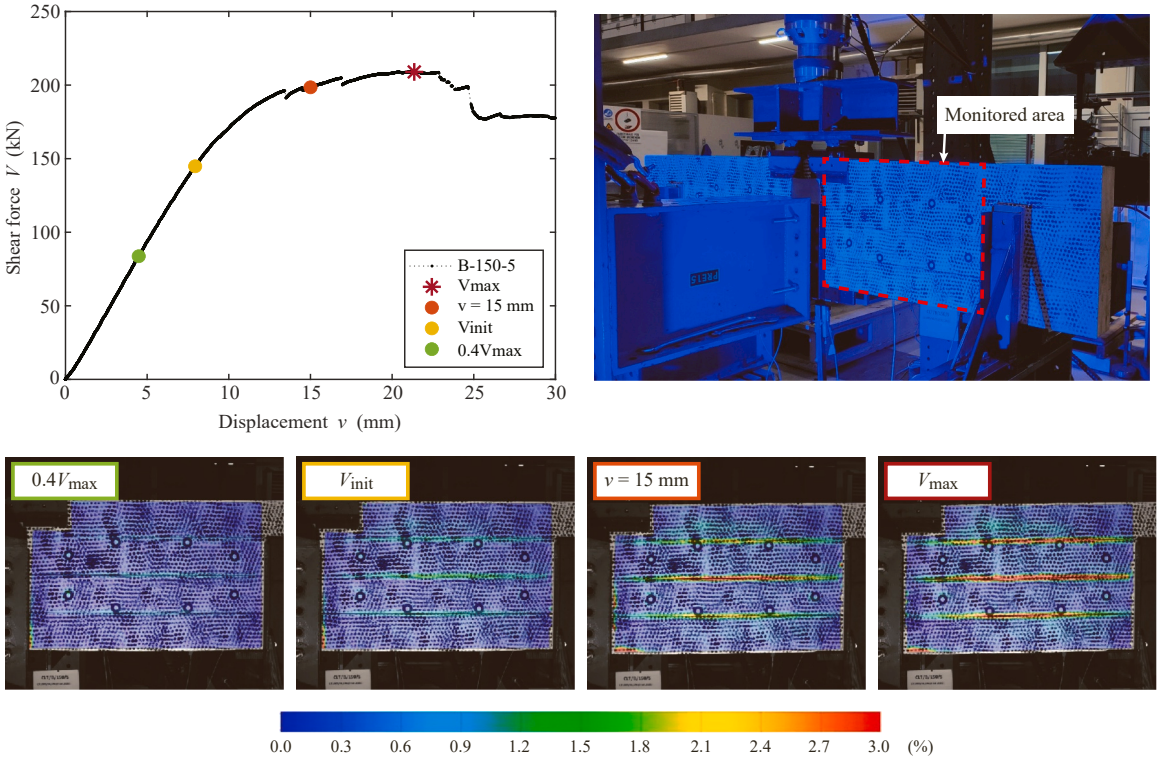

Fig. 8. Illustration of shear strains γ_{xy} from DIC measurements at four instants during testing (cf. the shear force vs. beam midspan displacement graph) for specimen B-150-5.

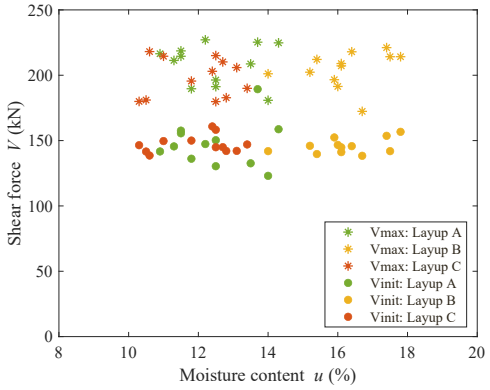

Fig. 9. Moisture content u versus maximum shear force (V_{max}) and shear force at initiation of nonlinear response (V_{init}) for all individual tests with results separated based on layup.

adjustments to a reference moisture content of 12% are used as well as results for shear forces V_{max} and V_{init} as given in Table 2.

For values adjusted to a moisture content of 12%, the maximum shear force $V_{max,12\%}$ for the 36 individual tests varied from 174.0 kN for test C-150-4 to 247.9 kN for test B-150-6, with an overall mean value of 210.9 kN and a coefficient of variation (CoV) of 9.1%. The six mean values (one per test series) of the maximum shear forces $V_{max,12\%}$ range from 191.5 kN for test series C-150 to 225.9 kN for test series B-100. This relatively small range of variation (± 10%) indicates an overall small influence of the individual lamination width $b = b_x = b_y$ and the ratio of the individual layer thicknesses $t_{x,2}/t_{x,1}$ on the maximum shear force V_{max}, which are the varying parameters between the six test series. The coefficients of variation (CoV) for $V_{max,12\%}$ for the three test series with lamination width $b = 100$ mm were 8.1%, 5.7% and 5.8% for layups A, B and C, respectively. The corresponding values for the test series with $b = 150$ mm were 7.5%, 9.8% and 8.9%.

Ratios between mean values of shear force levels V_{max}, $V_{max,12\%}$, V_{init} and $V_{init,12\%}$ for different test series and different subgroups of the tests are given in Table 3. The statistical significance of the differences between the test series was assessed using a two-sample t-test assuming unknown and unequal variances, with the null hypothesis that the samples of the compared test series originate from distributions with equal means. For comparisons of groups of tests which shows a statistically significant difference, the ratios are marked with an asterisk (*) in Table 3. At a significance level of 5%, the null hypothesis cannot be rejected if any combination of two of the six test series A-100, A-150, B-100, B-150, C-100, and C-150 (taking into account all six individual tests) is compared for either the V_{max} or V_{init} load level when using values which are not adjusted for variation in moisture content. This means that no significant statistical difference can be recognised when the test results for test series with different ratios $t_{x,2}/t_{x,1}$ or different lamination widths b are compared.

Using values $V_{max,12\%}$ and a significance level of 5%, the null hypothesis cannot be rejected when comparing two test series of equal layup (A, B or C, respectively) but with different lamination width ($b = 100$ mm

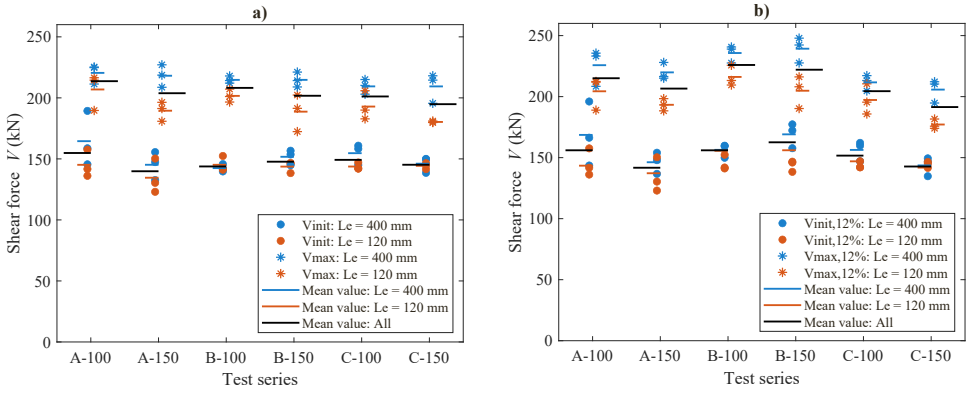

Fig. 10. Maximum shear force (V_{max}) and shear force at initiation of nonlinear response (V_{init}) for the six test series with results separated based on beam overhang at support (L_e). Values in a) refer to measured data according to Table 2 and values in b) refer to values adjusted to a reference moisture content of 12%.

Table 3
Ratios between mean values of shear force levels V_{max}, $V_{max,12\%}$, V_{init} and $V_{init,12\%}$ for different test series and different subgroups.

			Ratio between mean values of Group #1 and Group #2			
Group #1	vs.	Group #2	V_{max}	$V_{max,12\%}$	V_{init}	$V_{init,12\%}$
A-100		A-150	1.05	1.04	1.11	1.10
B-100		B-150	1.03	1.02	0.97	0.96
C-100		C-150	1.03	1.07	1.03	1.06 *
All, $b = 100$ mm		All, $b = 150$ mm	1.04	1.04	1.03	1.04
A-100		B-100	1.03	0.95	1.08	1.00
A-100		C-100	1.06	1.05	1.04	1.03
B-100		C-100	1.03	1.11 *	0.96	1.03
A-150		B-150	1.01	0.93	0.95	0.87 *
A-150		C-150	1.05	1.08	0.96	0.99
B-150		C-150	1.04	1.16 *	1.02	1.14 *
All, layup A		All, layup B	1.02	0.94	1.01	0.93
All, layup A		All, layup C	1.05	1.07	1.00	1.01
All, layup B		All, layup C	1.04	1.13 *	0.99	1.08 *
$b = 100$ mm, $L_e = 400$ mm		$b = 100$ mm, $L_e = 120$ mm	1.07 *	1.09 *	1.06	1.08
$b = 150$ mm, $L_e = 400$ mm		$b = 150$ mm, $L_e = 120$ mm	1.15 *	1.16 *	1.05	1.05
All, $L_e = 400$ mm		All, $L_e = 120$ mm	1.11 *	1.12 *	1.06 *	1.07 *

*Ratios representing statistically significant differences between mean values of the two groups, based on a two-sample t-test and a significance level of 5%.

and $b = 150$ mm). The same result is found for values of $V_{init,12\%}$ for layups A and B, but not for layup C. Based on the same type of comparison and considering equal lamination widths ($b = 100$ mm or $b = 150$ mm, respectively) but different layups (A, B and C), no statistical difference is found between layups A-B and A-C for the load level $V_{max,12\%}$. Considering the load level $V_{init,12\%}$, no statistical difference is found between layups A, B and C for test series with lamination width $b = 100$ mm. The same result is found for comparison between layups A and C for laminations width $b = 150$ mm, but not when comparing A to B or B to C.

For the two sets of 18 + 18 tests grouped by the overhang length, irrespective of the element layup and lamination width, the mean values of V_{max} are 214.5 kN for $L_e = 400$ mm and 193.3 kN for $L_e = 120$ mm, giving a ratio between the mean values as $V_{max,Le=400\ mm}/V_{max,Le=120\ mm} = 1.11$. The corresponding values for load level V_{init} are 150.8 kN for $L_e = 400$ mm and 142.8 kN for $L_e = 120$ mm, the corresponding ratio as 1.06. As can be seen in Table 3, very similar values are found for these two ratios between mean values also when considering the load levels $V_{max,12\%}$ and $V_{init,12\%}$. Using a two-sample t-test as described above, statistically significant differences are found when comparing the 18 tests with $L_e = 400$ mm with the 18 tests with $L_e = 120$ mm when considering any of the four load levels V_{max}, $V_{max,12\%}$, V_{init} and $V_{init,12\%}$.

The ratio between the mean value of the maximum load and the load at initiation of nonlinear response is greater for the beams with a long overhang compared to beams with a short overhang, with ratios as $V_{max,Le=400\ mm}/V_{init,Le=400\ mm} = 1.42$ and $V_{max,Le=120\ mm}/V_{init,Le=120\ mm} = 1.35$, both for unadjusted and adjusted results.

The load-bearing capacities $V_{max,12\%}$ and $V_{init,12\%}$ (based on adjustments to a reference moisture content of 12%) for the three different layups, with different relative longitudinal layer thicknesses are shown in Fig. 11. Predictions for shear force capacities according to Models 1, 2, and 3 (see Section 2.2) are also given in the figure, whereby the capacities are based on assumed mean strength values of $f_r = 1.5$ MPa and $f_{v,tor} = 3.5$ MPa.

The experimental results shown in Fig. 11 indicate that the element layup in terms of the ratio of the individual longitudinal layer thicknesses $t_{x,2}/t_{x,1}$ has a fairly small influence on the load-bearing capacity. Considering the maximum shear force $V_{max,12\%}$, the ratio $t_{x,2}/t_{x,1} = 1.0$ (layup B) shows the greatest shear force capacity for both lamination widths, $b = 100$ mm and $b = 150$ mm. Ratios $t_{x,2}/t_{x,1} = 0.5$ (layup A) and $t_{x,2}/t_{x,1} = 2.0$ (layup C) do however show very similar values for $V_{max,12\%}$ and $V_{init,12\%}$. Considering all three ratios $t_{x,2}/t_{x,1}$, it can be noted that Models 2 and 3 agree poorly with the experimental results, since these models predict an increasing shear force capacity with increasing ratio $t_{x,2}/t_{x,1}$. The overall trend of the experimental results is hence more consistent with the predictions of Model 1, showing no influence of the ratio $t_{x,2}/t_{x,1}$ on the shear force capacity.

Illustrations of the load-bearing capacity as influenced by the individual lamination width $b = b_x = b_y$ are shown in Fig. 12 for different layups in terms of the ratio between longitudinal layer thicknesses $t_{x,2}/t_{x,1}$ and considering load levels $V_{max,12\%}$ and $V_{init,12\%}$ as definitions of the capacity. Models 1–3 predict a strong influence of the lamination width b on the shear force capacity. However, the comparison of test series with different lamination widths b, and otherwise equal geometry indicates that there is no influence, neither at load level $V_{max,12\%}$ nor at load level $V_{init,12\%}$.

4. Discussion

The test results show very small or no significant influence of the element layup in terms of the ratio of the longitudinal layer thicknesses $t_{x,2}/t_{x,1}$ or the individual lamination width b on the load-bearing capacity. These two experimental results contradict the predictions of the load-bearing capacity with respect to shear failure mode III according to Models 2 and 3 in [20]. Model 1 according to Flaig & Blass [8,11] also does not agree with the experimental results regarding the influence of the lamination width b on the shear force capacity. Since Model 1 is based on the assumption of equal loading for all crossing areas in the direction of the beam width, regardless of the element layup, it does not predict any influence of the ratio of the longitudinal layer thicknesses $t_{x,2}/t_{x,1}$.

Model 3, which corresponds to the design proposal presented in [20],

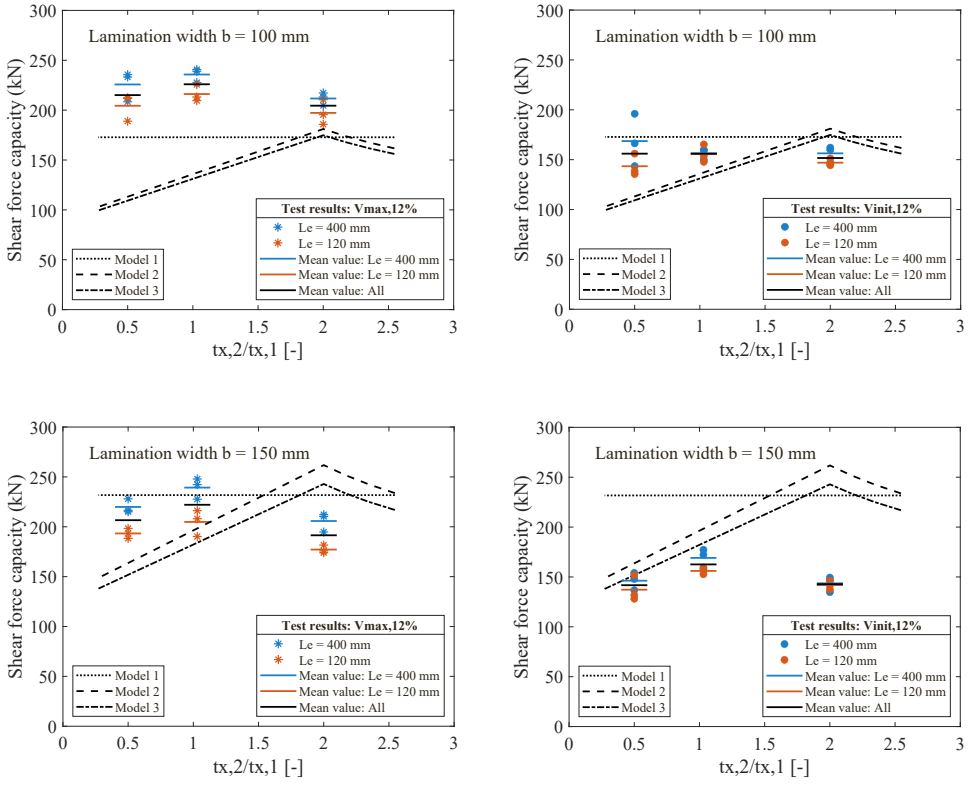

Fig. 11. Influence of relative longitudinal layer thickness on the shear force capacity for lamination width $b = 100$ mm (top) and $b = 150$ mm (bottom), based on $V_{max,12\%}$ (left) and $V_{init,12\%}$ (right).

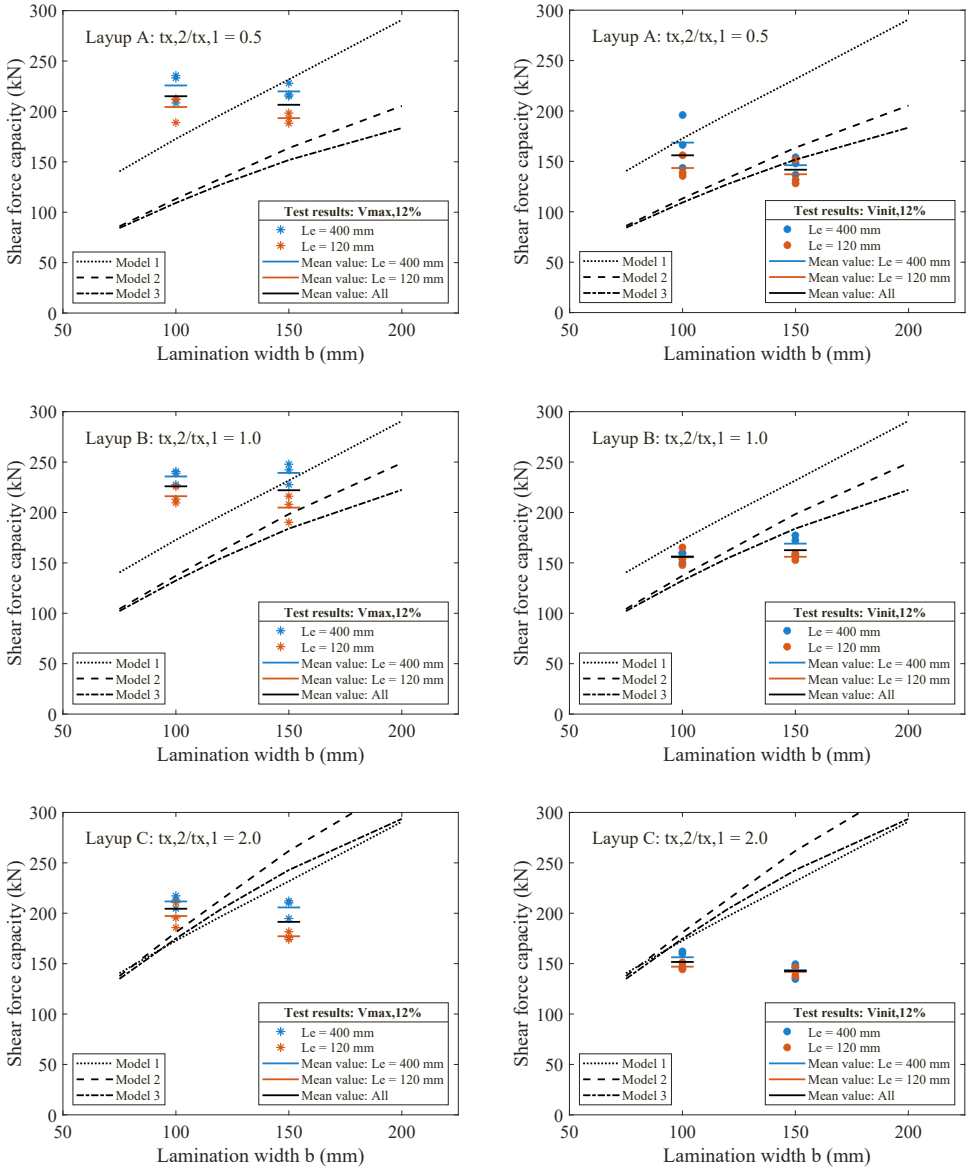

Fig. 12. Influence of lamination with b on the shear force capacity for layups A (top), B (middle) and C (bottom), based on $V_{max,12\%}$ (left) and $V_{init,12\%}$ (right).

generally provides the most conservative predictions of the three models considered. Compared to the mean values of the test results of the six test series with regards to the maximum shear force $V_{max,12\%}$, Models 2 and 3 provide conservative predictions for five of the six test series (see Figs. 11 and 12, with test series C-150 as the exception). The same conclusion is found when comparing mean values of test results without adjustments to the reference content of 12%.

The analytical models considered are all based on the assumption of linear elastic behaviour and shear stress distributions over the crossing areas as shown in Fig. 4. However, as can be seen in Figs. 5 and 6, the responses obtained in the tests are typically nonlinear. The global response in terms of shear force versus beam deflection at midspan (Fig. 5) shows a gradual decrease in stiffness before the maximum load is reached for most of the test. The gradual decrease in stiffness appears to be more pronounced in the test series with wide laminations, $b = 150$ mm, than in the test series with $b = 100$ mm laminations. The response in terms of shear force V in relation to the shear slip δ between the two centrally positioned longitudinal laminations (see Fig. 6) also shows a nonlinear behaviour with significant sliding before reaching the maximum load in many of the tests.

These two observations, the gradual decrease in overall stiffness after an initial linear phase, and the shear slip between the longitudinal laminations, can be explained by the loss of stiffness and the gradual damage to the bonding over the crossing areas between laminations of adjacent layers during loading. The reduction of stiffness in the initially highly stressed crossing areas leads to a redistribution of stress within the beam and, consequently, to increased stress in other crossing areas. This, in turn, leads to an increased bending effect of the individual longitudinal laminations. In later phases of loading, the interaction between laminations decreases and the laminations behave more like individual beams and not like laminations in a composite beam (where the cross-section remains plane under bending deformation). The final failure at, or after reaching, the maximum load can be described as bending failure of one or several laminations on the tension side of the beam.

The mean value of the maximum nominal normal stress σ_x varies between 29.2 and 31.8 MPa (see Table 2) for the six test series. Considerably greater values were found for the tests of CLT beams of similar size, layup and material quality – but with greater span-to-height-ratio – presented in [13,14]. For the test setup according to Figure A.1 e), mean values of the maximum normal stress σ_x at maximum load were found to be 39.7 MPa for beams with a longer span and 36.5 MPa for beams with a shorter span. A plausible explanation for

the significantly lower strength values obtained in the present tests is that failure mechanisms related to shear in the crossing areas have limited the load-bearing capacity.

Combined shear and compression perpendicular to the grain results in increased shear strength of timber and glulam beams, see e.g. [29] and [30]. This stress interaction effect is important in glulam and timber beams with a relatively short distance between a point load and a support, as is the case for the test configuration used in this paper. This effect should, however, be very small or negligible for CLT beams, since the loads and reaction forces are primarily transferred through the transverse layers due to the distribution being governed by the stiffness ratio of loading parallel and perpendicular to the grain. The magnitude of the compression stress perpendicular to the grain in the longitudinal layers close to supports and point loads is hence very small. The load transfer between longitudinal and transversal layers, over the bonding of the crossing areas, involves primarily longitudinal and rolling shear with little or no compression stress perpendicular to the crossing areas (and perpendicular to the grain in both longitudinal and transverse layers).

The shear stress distributions for single crossing areas loaded in uniaxial shear or torsion are discussed further in [31,32]. The 3D FE-analysis presented there showed spatially highly nonlinear shear stress distributions for the assumption of linear elastic behaviour, indicating that the shear stress distributions shown in Fig. 4 are rough approximations.

Of the three geometry parameters analysed, the length of the overhang at the support (L_e) appears to have the greatest influence on the experimentally determined load-bearing capacity considering maximum shear force during loading, see Fig. 10. One possible explanation is that the beam overhang (the extension beyond the line of action of the support reaction force) acts as a reinforcement by providing stiffness and preventing sliding between the longitudinal laminations of the same layer and preventing relative torsion between laminations of adjacent layers. As damage to the bonding over the crossing areas is initiated, the stiffness with respect to slip between longitudinal laminations and torsion between laminations of adjacent layers decreases. This leads to reduced composite action and the increased bending of the individual laminations, as mentioned above. The beam section extending beyond the line of action of the support reaction force, which according to conventional technical beam theory is mechanically inactive if the self-weight of the beam is disregarded, does however provide stiffness with respect to both these mechanisms, i.e. the relative sliding between longitudinal laminations and relative torsion between laminations of adjacent layers. An increased length of the beam overhang at the support should hence be beneficial in terms of load-bearing capacity. The influence of the overhang at the support cannot be captured by the analytical models considered, as they are based on beam theory considerations in which the stress state is determined by the beam cross-section forces at the location under consideration and assumption of a cross section which remains plane during bending deformation.

The values of net shear stress in the transverse layers $\tau_{xy,net}$ (related to shear FM II) range from 10.8 to 14.0 MPa for maximum loads V_{max} with no clear signs of net shear failure of the transverse laminations. Similar (and higher) values for net shear stress at maximum load for CLT beams are also reported in [2] and [13–15], with no apparent net shear failure. In [17], a characteristic net shear strength of $f_{v,xy,k} = 5.5$ MPa is proposed for CLT made from laminations of strength class T14 according to EN 338 [24]. However, for general safety reasons and considering the uncertainties in predicting the load-bearing capacity in relation to shear FM III, it may be appropriate to apply such a conservative value for the characteristic net shear strength. Assuming a mean value of the net shear strength as $f_{v,xy,mean} \approx 1.5 \cdot f_{v,xy,k} = 1.5 \cdot 5.5 = 8.25$ MPa and using Eq. (3) for determining the net shear stress in the transverse layers, the failure criterion $\tau_{xy,net} \leq f_{v,xy,mean}$ would give a predicted shear force capacity of $V = 132$ kN. This prediction of the capacity is lower than the maximum shear force (V_{max} or $V_{max,12\%}$) for all individual tests and lower than the initiation shear force (V_{init} or $V_{init,12\%}$) for 34 out of 36 specimens. It can hence be argued that a characteristic net shear strength of $f_{v,xy,k} = 5.5$ MPa is a reasonable choice regarding general safety aspects for design of CLT beams with respect to shear, considering shear failure modes II and III.

5. Conclusions

Experimental tests of 5-layer CLT under in-plane beam loading conditions were presented and from the results the following conclusions are drawn:

- The effective shear modulus, G_{ef}, was found to be greater for the beams with wide laminations ($b = 150$ mm) than for the beams with narrow laminations ($b = 100$ mm). The test results show no or only a small influence of the element layup in terms of the ratio $t_{x,2}/t_{x,1}$ on the effective shear modulus, and no influence of the length of overhang at the support.
- The capacity in terms of the maximum shear force (V_{max}, $V_{max,12\%}$)
  - o increases with increasing overhang length, in the present study the increase was on average 11–12% when the overhang changed from 120 mm to 400 mm.
  - o is not influenced by the width of the individual laminations ($b = b_x = b_y$).
  - o is influenced only to a small extent by the ratio the thickness of the longitudinal laminations ($t_{x,2}/t_{x,1}$).
- A possible reason for the discrepancies between model predictions and the test results is stress redistribution caused by gradual damage to the bonding between laminations of adjacent layers and partial mode III shear failure.
- The discrepancies between model predictions and load-bearing capacities according to tests motivates further research in this area, including investigation of the effect of the overhang in test situations, reconsideration of failure criteria and models for prediction of design-relevant stresses. It is crucial that such research efforts make use of models that can account for gradual damage evolution in the crossing areas, capturing the behaviour evidenced in this study in terms of large shear slips between laminations, and stress redistribution during loading.

CRediT authorship contribution statement

Boris Azinović: Writing – review & editing, Project administration, Methodology, Investigation, Funding acquisition, Data curation, Conceptualization. **Erik Serrano:** Writing – review & editing, Methodology, Funding acquisition, Conceptualization. **Tomaž Pazlar:** Writing – review & editing, Methodology, Investigation, Funding acquisition, Data curation, Conceptualization. **Henrik Danielsson:** Writing – review & editing, Writing – original draft, Methodology, Funding acquisition, Formal analysis, Conceptualization.

Declaration of Competing Interest

The authors declare that they have no known competing financial interests or personal relationships that could have appeared to influence the work reported in this paper.

Data Availability

Data will be made available on request.

Acknowledgement

The current research has received support for the project *InnoCrossLam* within ERA-NET Cofund ForestValue by MIZŠ, VINNOVA, FORMAS, STEM, BMLFUW, FNR and MINECO-AEI and has received funding from the European Union's Horizon 2020 research and innovation programme under grant agreement N° 773324. The financial support from FORMAS for the project *Strength and fracture analysis of cross laminated timber* (grant 2019-01354) and that from the Slovenian

Research Agency (Research Core Funding No. P2-0273 and P4-0430) is also gratefully acknowledged.

Appendix A

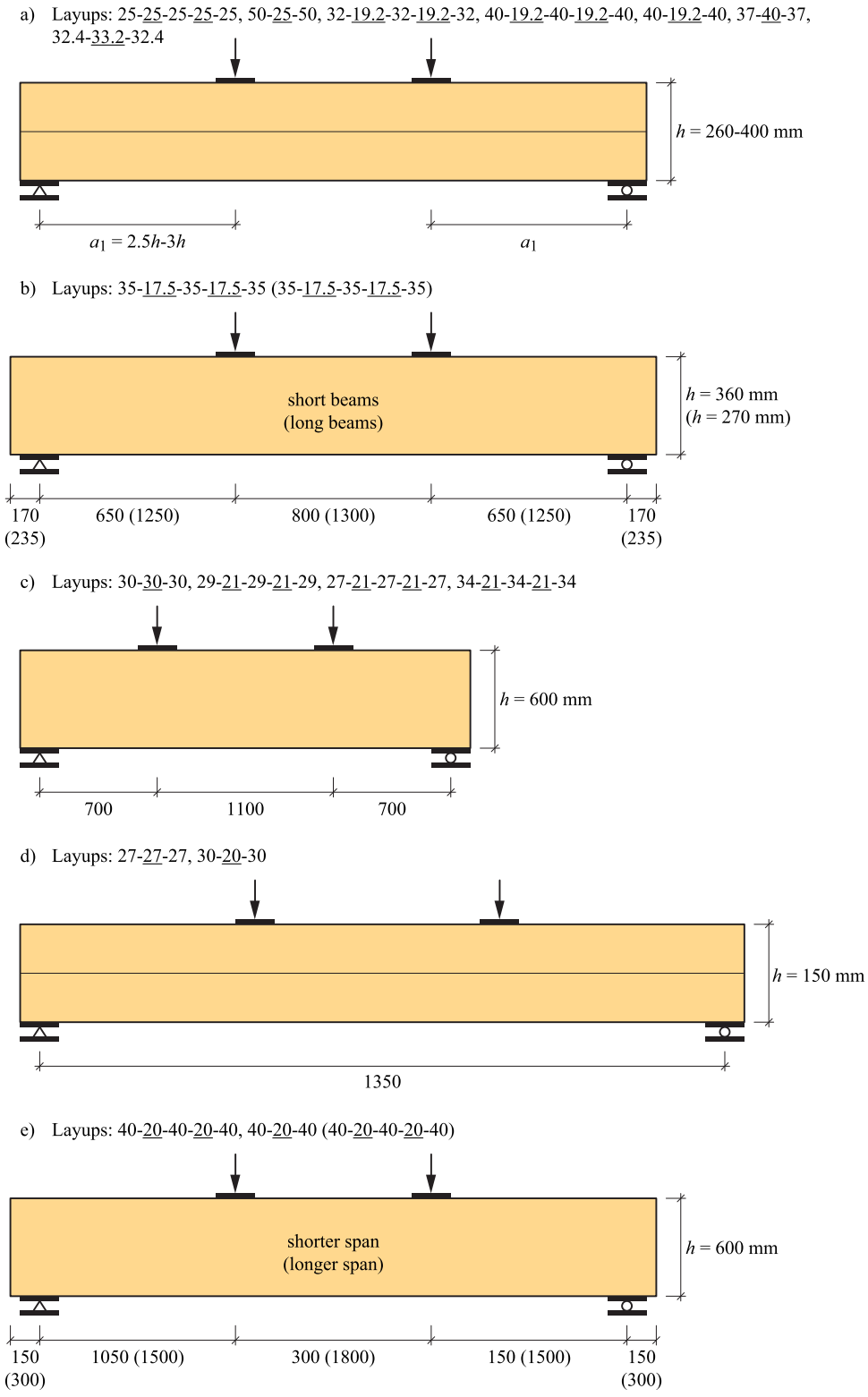

Figure A.1: Setups, beam geometries and layups used for experimental tests presented in: a) Jöbstl et al. [2], b) Bejtka [5], c) Andreolli et al. [6], d) Flaig [8] and Flaig & Blass [11], and e) Danielsson et al. [13,14] and Jeleč et al. [15]

.

References

[1] Danielsson H., Serrano E. In: Proc. INTER, INTER/52-12-2, Tacoma WA, USA; 2019.
[2] Jöbstl R.A., Bogensperger T., Schickhofer G. In-plane shear strength of cross laminated timber. In: Proc. CIB-W18, CIB-W18/41-12-3, St Andrews, Canada, 2008.
[3] CUAP Common Understanding of Assessment Procedure: Solid wood slab element to be used as a structural element in buildings. ETA request No 03.04/06, Österreichisches Institut für Bautechnik (OIB), Vienna, Austria; 2005.
[4] EN 408:2003. Timber structures – Structural timber and glued laminated timber – Determination of some physical and mechanical properties, CEN; 2003.
[5] Bejtka I. Cross (CLT) and diagonal (DLT) laminated timber as innovative material for beam elements. Karlsruhe, Germany: KIT; 2011.
[6] Andreolli M., Tomasi R., Polastri A. Experimental investigation on in-plane behavior of cross-laminated timber elements. In: Proc. CIB-W18, CIB-W18/45-12-4, Växjö, Sweden; 2012.
[7] EN 408:2010. Timber structures – Structural timber and glued laminated timber – Determination of some physical and mechanical properties, CEN; 2010.
[8] Flaig M. Biegeträger aus Brettsperrholz bei Beanspruch in Plattebene. PhD thesis, Karlsruhe, Germany: KIT; 2013.
[9] Flaig M. In Plattenebene beanspruchte Biegeträger aus Brettsperrholz – Teil 1: Effektive Festigkeits und Steifigkeitskennwerte für die Schubbemessung. Bautechnik 2015;92:741–9.
[10] Flaig M. In Plattenebene beanspruchte Biegeträger aus Brettsperrholz Teil 2: Brettsperrholzträger mit angeschnittenen Rändern, Durchbrüchen oder Ausklinkungen. Bautechnik 2015;92:750–8.
[11] Flaig M., Blass H.J. Shear strength and shear stiffness of CLT-beams loaded in plane. In: Proc. CIB-W18, CIB-W18/46-12-3, Vancouver, Canada; 2013.
[12] Flaig M., Blass H.J. Bending strength of cross laminated timber loaded in plane. In: Proc. WCTE 2014, Quebec City, Canada; 2014.
[13] Danielsson H., Jeleč M., Serrano E. Strength and stiffness of cross laminated timber at in-plane beam loading. Report TVSM-7164, Division of Structural Mechanics, Lund University, Sweden; 2017.
[14] Danielsson H., Serrano E., Jeleč M., Rajčić V. In-plane loaded CLT beams – Tests and analysis of element lay-up. In: Proc. INTER, INTER/50-12-2, Kyoto, Japan; 2017.
[15] Jeleč M, Danielsson H, Rajčić V, Serrano E. Experimental and numerical investigations of cross laminated timber at in-plane beam loading conditions. Constr Build Mater 2019;206:329–46.
[16] Karacabeyli E., Gagnon S. Canadian CLT Handbook 2019 Edition, Special Publication SP-532E, FPInnovations, 2019.
[17] Brandner R, Tomasi R, Moosbrugger T, Serrano E, Dietsch P. Properties, testing and design of cross laminated Timber (eds). A state-of-the-art report by COST Action FP1402/WG2. Aachen, Germany: Shaker Verlag; 2018.
[18] CEN/TC 250. Draft prEN 1995–1-1:2023(E), Eurocode 5 – Design of timber structures – Part 1–1: General rules and rules for buildings, September 2023.
[19] Danielsson H, Jeleč M, Serrano E, Rajčić V. Cross laminated timber at in-plane beam loading – Comparison of model predictions and FE-analysis. Eng Struct 2019; 179:246–54.
[20] Danielsson H, Jeleč M. A unified design proposal for shear stress prediction in crossing areas for cross laminated timber at in-plane shear and beam loading conditions. Constr Build Mater 2022;355:129167.
[21] Danielsson H, Serrano E. Cross laminated timber at in-plane beam loading – Prediction of shear stresses in crossing areas. Eng Struct 2018;171:921–7.
[22] Danielsson H., Jeleč M., Serrano E. Prediction of torsional stress at in-plane shear loading of cross laminated timber. In: Proc. INTER, INTER/53-12-3, Online Meeting; 2020.
[23] Allgemeine bauaufsichtliche Zulassung / Allgemeine Bauartgenehmigung. Nummer Z-9.1–555. LIGNOTREND-Elemente in tragenden Wand-, Decken- und Dachkonstruktionen, LIGNOTREND GmbH & Co. KG. Deutsches Institut für Bautechnik. https://www.dibt.de/de/service/zulassungsdownload/detail/z-91–555.
[24] EN 338. Structural timber – Strength classes, CEN; 2016.
[25] EN 13183–2. Moisture content of a piece of sawn timber – Part 2: Estimation by electrical resistance method, CEN; 2002.
[26] EN 408:2010+A1:2012. Timber structures – Structural timber and glued laminated timber – Determination of some physical and mechanical properties, CEN; 2012.
[27] Brandner R., Getternig W., Schickhofer G. Determination of shear strength of structural and glued laminated timber. In: Proc. CIB-W18, CIB-W18/45-12-2, Växjö, Sweden, 2012.
[28] Akter ST, Binder E, Bader TK. Moisture and short-term time-dependent behavior of Norway spruce clear wood under compression perpendicular to the grain and rolling shear. Wood Mater Sci Eng 2023;18(2):580–93.
[29] Crocetti R., Gustafsson P.J., Danielsson H., Emilsson A., Ormarsson S. Experimental and numerical investigation on the shear strength of glulam. In: Proc. CIB-W18, CIB-W18/43-12-2, Nelson, New Zealand, 2010.
[30] Steiger R., Gehri E. Interaction of shear stresses and stresses perpendicular to the grain. In: Proc. CIB-W18, CIB-W18/44-6-2, Alghero, Italy, 2011.
[31] Danielsson H., Serrano E. Cross laminated timber at in-plane shear loading – Strength and fracture analysis of shear mode III. In: Proc. WCTE, Santiago, Chile, Online; 2021.
[32] Danielsson H., Serrano E. Shear failure mechanism III in cross laminated timber – Numerical investigations of fracture behaviour. In: Proc. WCTE, Oslo, Norway; 2023.